

FERMI constraints on the high energy, $\sim 1\text{GeV}$, emission of long GRBs

Dafne Guetta¹, Elena Pian^{2,3,4} and Eli Waxman⁵

¹ Osservatorio astronomico di Roma, v. Frascati 33, 00040 Monte Porzio Catone, Italy

² Osservatorio Astronomico di Trieste, Via G.B. Tiepolo, 11 - 34143 Trieste, Italy

³ Scuola Normale Superiore, Piazza dei Cavalieri 7, I-56126 Pisa, Italy

⁴ European Southern Observatory, Karl-Schwarzschild-Strasse 2 D-85748 Garching bei München, Germany

⁵ Dept. of Particle Phys. & Astrophys., Weizmann Institute of Science, Rehovot 76100, Israel

Preprint online version: June 15, 2018

ABSTRACT

Aims. We investigate the constraints imposed on the luminosity function (LF) of long duration Gamma Ray Bursts (LGRBs) by the flux distribution of bursts detected by the GBM at $\sim 1\text{ MeV}$, and the implications of the non detection of the vast majority, $\sim 95\%$, of the LGRBs at higher energy, $\sim 1\text{ GeV}$, by the LAT detector.

Methods. We find a LF that is consistent with those determined by BATSE and *Swift*. The non detections by LAT set upper limits on the ratio R of the prompt fluence at $\sim 1\text{ GeV}$ to that at $\sim 1\text{ MeV}$. The upper limits are more stringent for brighter bursts, with $R < \{0.1, 0.3, 1\}$ for $\{5, 30, 60\}\%$ of the bursts. This implies that for most bursts the prompt $\sim 1\text{ GeV}$ emission may be comparable to the $\sim 1\text{ MeV}$ emission, but can not dominate it. The value of R is not universal, with a spread of (at least) an order of magnitude around $R \sim 10^{-1}$. For several bright bursts with reliable determination of the photon spectral index at $\sim 1\text{ MeV}$, the LAT non detection implies an upper limit to the $\sim 100\text{ MeV}$ flux which is < 0.1 of the flux obtained by extrapolating the $\sim 1\text{ MeV}$ flux to high energy.

Results. For the widely accepted models, in which the $\sim 1\text{ MeV}$ power-law photon spectrum reflects the power-law energy distribution of fast cooling electrons, this suggests that either the electron energy distribution does not follow a power-law over a wide energy range, or that the high energy photons are absorbed. Requiring an order unity pair production optical depth at 100 MeV sets an upper limit for the Lorentz factor, $\Gamma \lesssim 10^{2.5}$.

Key words. gamma rays: bursts

1. Introduction

Gamma ray bursts (GRBs) are the most powerful explosions in the universe, with apparent (isotropic equivalent) energy output sometimes exceeding 10^{54} ergs . While it is widely accepted that GRBs are produced by the dissipation of energy in highly relativistic winds driven by compact objects (see, e.g., Mészáros 2006, Piran 2004 and Waxman 2003 for reviews) the physics of wind generation and radiation production is not yet understood. It is not known, for example, whether the wind luminosity is carried, as commonly assumed, by kinetic energy or by Poynting flux (e.g. Drenkhahn & Spruit 2002, Lyutikov et al. 2003), whether the radiating particles are accelerated by the dissipation of magnetic flux or by internal shocks dissipating kinetic energy, and whether the emission is dominated by synchrotron or inverse-Compton radiation of accelerated electrons, as commonly assumed, or by hadronic energy loss of accelerated protons (see Dermer & Fryer 2008 and references therein).

GRBs were detected by instruments sensitive mainly in the 100 to 1000 keV range like BATSE (Paciesas et al. 1999) and the GRBM on BeppoSAX (Guidorzi et al. 2004). Measurements at high energy were limited by the lower sensitivity and/or the smaller field of view of higher energy instruments (e.g. CGRO/EGRET-Dingus 1995, Hurley et al. 1994, Gonzalez et al. 1994; AGILE/GRID-Marisaldi et al. 2009, Giuliani et al. 2008, Giuliani et al. 2010). The improved high energy, $\gtrsim 1\text{ GeV}$, sensitivity and field of view of the instruments on board the Fermi satellite (Atwood et al. 2009, Band et al. 2009) are expected to

improve the quantity and quality of high energy GRB data, and may therefore provide qualitatively new constraints on models.

The main goal of this paper is to determine the implications of the non-detection of the vast majority of long duration ($T > 2\text{ s}$) GRBs by Fermi's LAT detector. We first show in § 2 that the LF of LGRBs detected by Fermi's GBM at $\sim 1\text{ MeV}$ is consistent with those inferred from BATSE and *Swift* observations, and that these instruments sample the LF in a similar manner. We then derive in § 3 the constraints on the $> 100\text{ MeV}$ emission implied by LAT non-detections. In § 4 we compare our results with those inferred from the analysis of EGRET data (Gonzalez Sanchez 2005). Our results are summarized and their implications are discussed in § 5.

2. The luminosity function of the GBM sample

2.1. The GBM, BATSE and *Swift*-BAT samples

Our methodology follows that of Guetta et al. (2005) and of Guetta & Piran (2007). We consider all long ($T_{90} > 2\text{ seconds}$) bursts detected by the GBM until February 2010 (see Table 2) and compare the distribution of their peak fluxes with that of LGRBs detected by BATSE and *Swift*. Since the energy dependent sensitivity of the different instruments is different, we convert the GBM fluxes to equivalent fluxes in the 50-300 keV band, which is the band used by BATSE for GRB triggers. This conversion is carried out assuming that the energy spectrum around the light curve peak is well described by the spectral model that

has been adopted to fit the time average spectrum. The spectral model parameters have been collected from the literature (mainly GCN circulars) and are reported in Table 2.

We have excluded from our analysis GRB081126, which has 2 pulses, because the measurements reported in GCN 8589 are inconsistent: the peak flux and fluence of the event are reported to be smaller than those reported for the individual pulses. We have kept GRB090423 in our analysis, despite the debate regarding its classification as a long burst (see Salvaterra et al. 2009) since its duration does satisfy $T_{90} > 2$ s.

For bursts reported in Table 2 with spectra fitted by a "Band law", $dN_\gamma/dE \propto E^\alpha$ for $E < E_p$ and $dN_\gamma/dE \propto E^\beta$ for $E > E_p$, we find $\langle \alpha \rangle \approx -0.8$, $\langle \beta \rangle \approx -2.3$, and $\langle E_p \rangle \approx 200$ keV. Using these average parameters, we estimate, based on Band (2003), a GBM sensitivity in the 50-300 keV band of $P_{\text{lim,GBM}}^{(50-300)\text{keV}} \sim 0.6 \text{ ph cm}^{-2} \text{ s}^{-1}$. For our LF analysis we use only the 144 long ($T_{90} > 2$ s) GBM bursts with peak flux higher than that threshold.

In the BATSE sample we have included all LGRBs detected while the BATSE onboard trigger was set to a significance of 5.5σ over background in at least two detectors in the energy range of 50-300 keV. Among those we selected the bursts for which the peak flux in 1024 ms time bins is higher than the BATSE threshold for long bursts reported by Band (2003), $P_{\text{lim,BATSE}}^{(50-300)\text{keV}} \sim 0.25 \text{ ph cm}^{-2} \text{ s}^{-1}$. This yields a sample of 1425 bursts.

For *Swift* we consider LGRBs detected until September 2009 in the energy range 15-150 keV. We convert the BAT 15-150 keV peak fluxes to fluxes in the 50-300 keV band using the BAT peak fluxes and spectral parameters provided by the *Swift* team¹. We consider only the bursts with peak fluxes above the threshold of $P_{\text{lim,Swift}}^{(50-300)\text{keV}} \sim 0.3 \text{ ph cm}^{-2} \text{ s}^{-1}$ (Gorosabel et al. 2004, Band 2003), yielding a sample of 259 GRBs.

The flux distributions of bursts included in the samples described above are shown in figure 1.

2.2. Luminosity function and comoving rate

The method used to derive the luminosity function is essentially the same as that used by Schmidt (1999), Guetta et al. (2005) and Guetta and Piran (2007). We consider a broken power law luminosity function,

$$\Phi(L) \equiv \frac{dN}{d \log L} \propto \begin{cases} (L/L^*)^{-a_1} & L^*/\Delta_1 < L < L^* \\ (L/L^*)^{-a_2} & L^* < L < \Delta_2 L^* \end{cases}, \quad (1)$$

with $\Delta_1 = 100$, $\Delta_2 = 100$ and $\{L^*, a_1, a_2\}$ independent of redshift, and a (comoving) rate evolving with redshift following the Porciani & Madau (2001) star formation rate,

$$R_{GRB}(z) \propto \frac{\exp(3.4z)}{\exp(3.4z) + 22}. \quad (2)$$

The cosmological "k correction" is determined adopting an effective spectral index in the observed range of 50-300 keV band of -1.6 ($dN_\gamma/dE \propto E^{-1.6}$) (see, e.g., Guetta and Piran 2007).

In order to determine $\{L^*, a_1, a_2\}$ we use Monte Carlo simulations to generate an ensemble of distributions of burst peak fluxes, that would have been detected by the various instruments for a given set of $\{L^*, a_1, a_2\}$ values. We find the best-fitting LF parameters $\{L^*, a_1, a_2\}$ and their uncertainty by χ^2 minimization.

¹ See *Swift* information page
http://Swift.gsfc.nasa.gov/docs/Swift/archive/grb_table.html

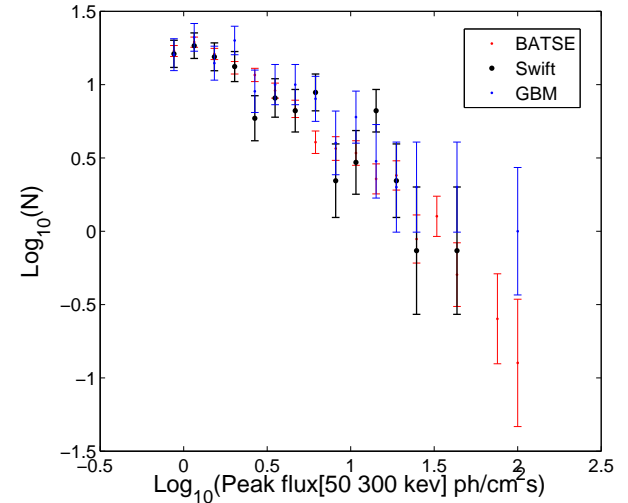


Fig. 1. The flux distributions of bursts included in the BATSE, *Swift* and GBM samples (see text). Shown are the number of bursts detected within 20 equally spaced intervals of log peak flux (in the 50-300 keV band). Error bars derived assuming Poisson statistics.

The results are reported in Table 1. The LF parameters derived from the different samples are consistent with each other. Note, that the luminosity considered here is the "isotropic" equivalent luminosity.

Table 1. Best fit LF parameters¹

sample	Rate(z=0) ⁽¹⁾ Gpc ⁻³ yr ⁻¹	L^* [50-300] keV 10 ⁵¹ erg/s	a ₁	a ₂	$\chi^2/\text{D.O.F.}^{\text{(3)}}$
GBM	$0.5^{+0.3}_{-0.2}$	$5.5^{+1.5}_{-2}$	$0.3^{+0.1}_{-0.3}$	$2.3^{+0.6}_{-0.3}$	1.1
BATSE	$1.0^{+0.2}_{-0.4}$	$4^{+2}_{-1.5}$	$0.1^{+0.3}_{-0.1}$	$2.6^{+0.8}_{-0.5}$	1.1
Swift	$0.6^{+0.4}_{-0.1}$	$3.3^{+2.5}_{-0.5}$	$0.1^{+0.3}_{-0.1}$	$2.7^{+1}_{-0.4}$	0.95

Notes. ⁽¹⁾ Best fit values and their 1σ uncertainty range.

⁽²⁾ Integrated over L .

⁽³⁾ χ^2 obtained for best fit values.

3. Constraints on the > 100 MeV emission implied by LAT non-detections

Out of the 205 LGRBs detected by the GBM, only a few, ~ 12 bursts, have been detected above 30 MeV by the LAT telescope. Figures 2 and 3 present the upper limits implied by the LAT non-detection on the ratio of the prompt emission fluences at 100 MeV and 1 MeV. We have included in the burst sample shown in the figure the 121 LGRBs for which an accurate determination of the 1 MeV fluence is possible based on the fluence measured by the Fermi GBM and on reliable spectral fit

parameters (see table 2)^{2,3,4}, and for which the reported LAT bore sight angle is less than 80° (as the LAT effective area is very small for bursts observed at larger angles). The upper limit on the > 100 MeV fluence implied by the LAT non-detection is derived as follows.

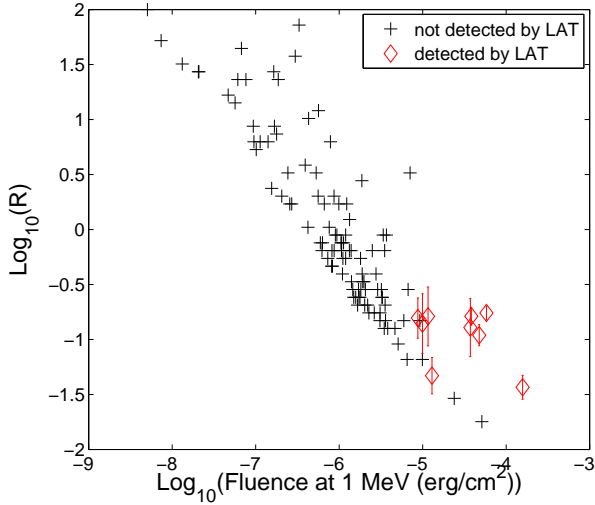


Fig. 2. The upper limits implied by the LAT non-detections on the ratio R of the 100 MeV to 1 MeV fluences, $vF_v = v \int dt f_v(t)$ for $hv = 1, 100$ MeV, during the prompt emission, assuming a differential photon spectrum $dN_\gamma/dE \propto E^{-2}$ above 100 MeV. Also shown (red diamonds) are the measured ratios for GRBs detected by the LAT (GRB080825C, GRB080916C, GRB090217, GRB090323, GRB090328, GRB090626, GRB090902B, GRB090926A, GRB091003, reported in Ghisellini et al. 2010 and Abdo et al. 2010). The 100 MeV specific fluence was derived for these bursts from the reported > 100 MeV fluence assuming $dN_\gamma/dE \propto E^{-2}$ above 100 MeV.

A GRB is tagged as detected by the LAT if the number of photons detected, N_s , exceeds 10 and exceeds a 5σ fluctuation of the background (Band et al. 2009, Atwood et al. 2009). For the current analysis, it is sufficient to consider the $N_s > 10$ criterion, since the number of background events detected during the characteristic time of the prompt ~ 1 MeV gamma-ray emission, $T_{90} \lesssim 100$ s, is low (~ 1 , i.e. $N_s > 10$ is above a 5σ background fluctuation). Following Band et al. (2009), the expected number

² Some GRBs have reported fluence and no reported peak flux. While these GRBs were excluded from the peak flux analysis described in § 2, they have been included in the fluence ratio analysis.

³ For 4 GRBs with multi-peak structure, separate sets of spectral fit parameters are reported in the literature for each pulse (GRBs 081009, 090509, 090516A, 090610B). In these cases, we have determined the 1 MeV fluence using the spectrum of the second pulse (see Table 2), under the assumption that the bulk of the MeV-GeV output is emitted simultaneously with the second pulse. This is motivated by the 2 long GRBs with detailed published GBM and LAT light curves, GRB080916C (Abdo et al. 2009) and GRB090902B (Bissaldi et al. 2009).

⁴ For GRBs with spectra fitted in the GBM band with single power-laws, the spectrum cannot be extrapolated straightforwardly to 1 MeV if the energy range used for the power-law fit is much softer. Thus, we have retained the GRBs fitted with single power-laws over an energy reaching or exceeding 800 keV, and excluded from the analysis GRBs 080818A, 080928, 081206C, 081225.

of counts from a burst with a time integrated differential photon flux (i.e. differential photon fluence) $Q(E)$ is

$$N_S = \int_{E_1}^{E_2} dE A_{eff}(E, \theta) Q(E), \quad (3)$$

where $A_{eff}(E, \theta)$ is the effective area (taken from Atwood et al. 2009) that depends on the direction from which the burst is observed, θ , $E_1 = 100$ MeV and $E_2 = 10$ GeV.

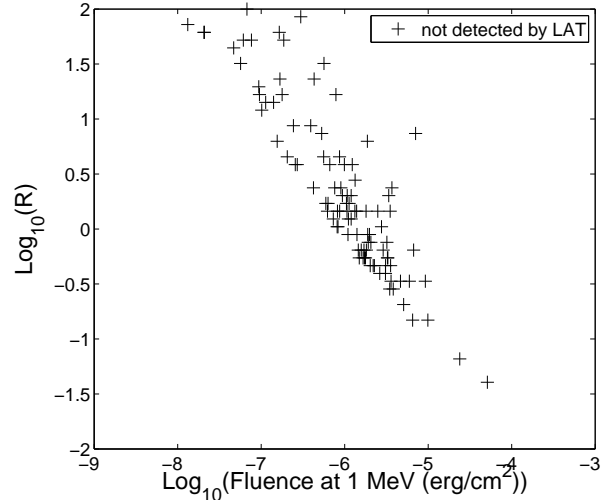


Fig. 3. Same as figure 2, assuming a differential photon spectrum $dN_\gamma/dE \propto E^{-3}$ above 100 MeV.

The upper limits on the 100 MeV fluences shown in figures 2 and 3 are obtained by requiring $Q(E) < Q_0(E)$ where $Q_0(E)$ is the fluence for which $N_s = 10$. Since the number of events detected for bursts with fluence that produces, on average, $N_s = 10$ events is Poisson distributed with an average equal to 10, the upper limits on the fluxes shown in the figure are $\sim 50\%$ confidence level upper limits. The upper limits on the fluence for confidence levels of 70% and 99.7% are 1.2 and 2 times higher respectively.

The effective area of the LAT is roughly proportional to E in the energy range of 100 MeV to 1 GeV (and roughly energy independent between 1 GeV and 10 GeV). This implies that the LAT flux sensitivity is roughly energy independent between 100 MeV and 1 GeV, and that the upper limit on N_s implies an upper limit on the 0.1–1 GeV fluence, which is independent of the spectrum $Q(E)$. Indeed, the upper limits on R , the 100 MeV to 1 MeV fluence ratio, obtained assuming $Q(E) \propto E^{-3}$ are higher by a factor of ~ 2 than those obtained for a $Q(E) \propto E^{-2}$, implying that the upper limits on the 0.1–1 GeV fluence obtained for both spectral shapes are similar. Denoting by $R^{(2)}$ the upper limit obtained on R assuming $Q(E) \propto E^{-2}$, the upper limit on the 0.1–1 GeV fluence is $\approx \ln(10)R^{(2)}vF_v|_{1\text{MeV}}$, the upper limit on the 1–10 GeV fluence is few times higher, and the upper limit on the ratio of the 0.1–1 GeV fluence and the 0.1–1 MeV fluence is $\approx R^{(2)}$. We find $R^{(2)} < \{0.1, 0.3, 1\}$ for $\{5, 30, 60\}\%$ of the bursts respectively. Figure 4 presents a histogram of the distribution of upper limits on $R^{(2)}$.

In figure 5 we present the upper limits implied by the LAT non-detection on the ratio S between the 100 MeV fluence and the 100 MeV fluence obtained by extrapolation to 100 MeV of the ~ 1 MeV spectrum of the GBM detected photons. For this comparison, we have used only the ~ 60 bursts with spectra

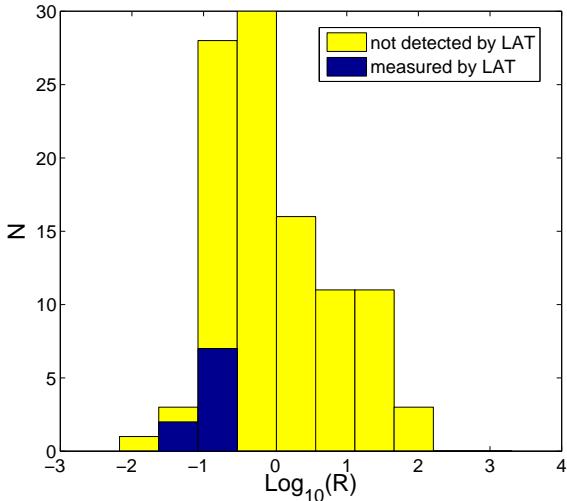


Fig. 4. A histogram representation of the upper limits on, and measured values of, R , presented in fig. 2.

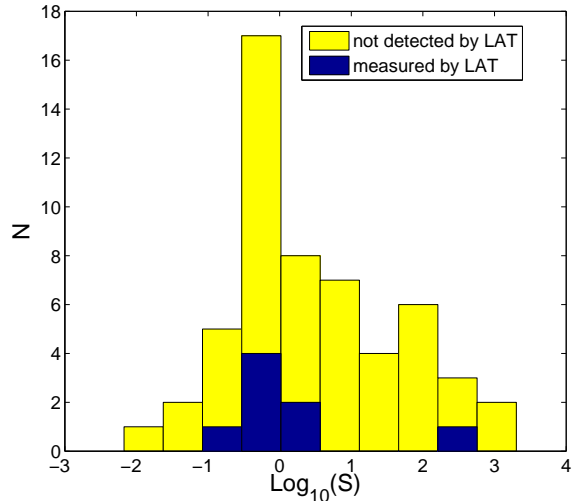


Fig. 6. A histogram representation of the results of fig. 5.

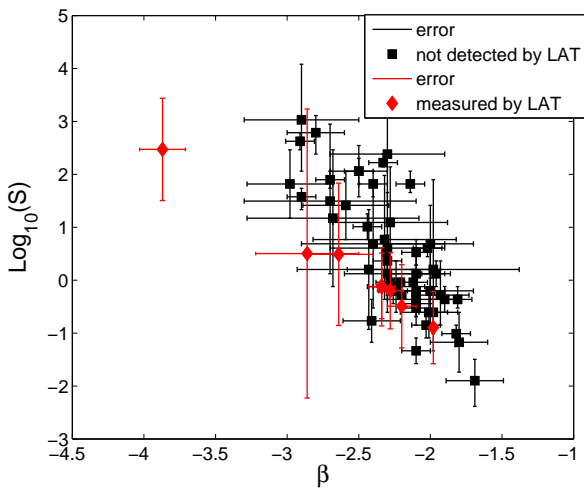


Fig. 5. Upper limits implied by LAT non-detections on the ratio S between the 100 MeV fluence and the 100 MeV fluence obtained by extrapolation to 100 MeV of the ~ 1 MeV spectrum of the GBM detected photons. β is the spectral index describing the high energy part of the GBM spectrum, $dN_\gamma/dE \propto E^\beta$. Also shown are the measured values of S for LAT detected GRBs (red).

which are well fitted by a "Band function" and for which the bore sight angle is $< 80^\circ$. We have excluded from the sample shown in the figure bursts for which the GBM spectrum is not fitted by a Band law, i.e. fitted by either a power-law with exponential suppression (which predicts negligible flux at 100 MeV) or by a single power-law (for which a spectral break above 1 MeV is not unexpected). A histogram representation of the results of fig. 5 is shown in fig. 6. The figures show that for at least a few bursts the non detection by LAT implies a significant suppression of the 100 MeV flux compared to that expected from an extrapolation to high energy of the ~ 1 MeV power-law spectrum.

4. Comparison with EGRET's results

We compare in this section our results with those obtained by González Sánchez (2005) and Ando et al. (2008) from the non detection by EGRET of bursts detected by BATSE. EGRET detected photons in the 30 MeV-30 GeV energy range, with effective area roughly proportional to E between 30 MeV and 200 MeV, and approximately energy independent ($\approx 10^3 \text{ cm}^2$) at higher energy (see Thompson et al. 1993). This area is similar to the LAT effective area at ~ 100 MeV and smaller by roughly an order of magnitude than the LAT effective area at ~ 1 GeV. From table 2.1 and fig. 2.3 of González Sánchez (2005), EGRET's non-detections imply upper limits on the ratio of the EGRET fluence to the 20 keV-1 MeV BATSE fluence of $\approx 5\%$ (consistent with Ando et al. 2008) for the brightest available bursts ($50\text{-}300$ keV BATSE fluence $> 10^{-5} \text{ erg/cm}^2$), and much weaker, ≈ 1 , for dimmer bursts.

The roughly linear dependence of EGRET's effective area between 30 MeV and 200 MeV, and the energy independent area at higher energy, implies that EGRET's flux sensitivity is roughly energy independent between 30 MeV and 200 MeV, and falling at higher energy. Combined with the fact that the upper limits reported in González Sánchez (2005) were obtained assuming a $dN_\gamma/dE \propto E^{-2.4}$ spectrum, these upper limits apply to the 30 MeV-200 MeV fluence (the constraint implied on the fluence at higher energy is weaker and depends on the assumed spectrum). The upper limits derived in § 3 using LAT non-detections on the 0.1-1 GeV fluence are similar to those obtained by EGRET on the 30 MeV-200 MeV fluence. We obtained $R^{(2)} < 0.1$ for the brightest $\sim 5\%$ of the bursts, and $R^{(2)} < 3\%$ for the brightest in the sample (GRB081207 and GRB090829A), see fig. 2.

5. Summary and discussion

We have shown that the LGRB LF inferred from the sample of bursts detected by Fermi's GBM is consistent with those determined by BATSE and *Swift*, see table 1, and that the GBM samples this LF in a manner similar to that of BATSE & *Swift*, see figure 1. We have derived the upper limits implied by the LAT non-detections on the ratio R of the 100 MeV to 1 MeV fluences, $\nu F_\nu = \nu \int dt f_\nu(t)$ for $h\nu = 1, 100$ MeV, during the

prompt emission. The upper limits on R obtained assuming $dN_\gamma/dE \propto E^{-2}$ at $E > 100\text{ MeV}$ (see fig. 2), also imply upper limits on the 0.1–1 GeV fluence, which is approximately given by $\ln(10)R\nu F_\nu|_{1\text{MeV}}$ (the upper limit on the 1–10 GeV fluence is few times higher and depends on the assumed spectrum), and on the ratio of the 0.1–1 GeV fluence and the 0.1–1 MeV fluence, which is $\approx R$. The upper limits on R are more stringent for brighter bursts (see fig. 2), with $R < \{0.1, 0.3, 1\}$ for $\{5, 30, 60\}\%$ of the bursts (see fig. 4). This implies that for most bursts the prompt $\sim 1\text{ GeV}$ emission may be comparable to the $\sim 1\text{ MeV}$ emission, but can not dominate it. For several bright bursts with reliable determination of the photon spectral index at $\sim 1\text{ MeV}$, the LAT non detection implies an upper limit to the $\sim 100\text{ MeV}$ flux which is < 0.1 of the flux obtained by extrapolating the $\sim 1\text{ MeV}$ flux to high energy (see fig. 5). Examining figs. 2 and 4, we conclude that the ratio R is not universal among GRBs. The detections and non-detection upper limits imply a spread in R over at least an order of magnitude. The upper limits we obtain are similar to those inferred for the fluence at lower energy, 30–200 MeV, from EGRET’s non-detections of BATSE bursts (see § 4).

The upper limits on R provide constraints on models for the prompt GRB emission. Models where the prompt $\sim 1\text{ MeV}$ emission is produced by inverse-Compton scattering of optical synchrotron photons (e.g. Stern & Poutanen 2004, Panaitescu & Kumar 2007), typically predict $R \geq 1$. This is not supported by the data. Such models are not necessarily ruled out by the current data, as they might be modified to include a suppression of the $\sim 1\text{ GeV}$ flux by pair production. Such modification may be required for all (widely discussed) models, in which the $\sim 1\text{ MeV}$ power-law photon spectrum reflects the power-law energy distribution of fast cooling electrons. The suppression of the $\sim 100\text{ MeV}$ flux, compared to that expected from an extrapolation of the $\sim 1\text{ MeV}$ power-law spectrum, suggests that either the electron energy distribution does not follow a power-law over a wide energy range, or that the high energy photons are absorbed, probably by pair production. Requiring an optical depth of ~ 1 at 100 MeV sets an upper limit to the expansion Lorentz factor $\Gamma \lesssim 10^{2.5}[(L/10^{52}\text{erg/s})/(t_v/10\text{ ms})]^{1/6}$ (e.g. eq. 7 of Waxman 2003). Significant compactness of the emission region has been suggested by several authors (e.g. Guetta et al. 2001, Pe’er & Waxman 2004). The spectrum is modified in this case, compared to the optically thin case, with 100 MeV to 1 MeV flux ratios in the range $0.01 \lesssim R \lesssim 0.1$ obtained for typical parameters (e.g. figs. 8 & 11 of Pe’er & Waxman 2004).

Acknowledgements. This research was supported in part by ISF, AEC and Minerva grants. DG & EP thank the Benoziyo center for Astrophysics at the Weizmann institute for hospitality during the time at which this research was initiated. We thank Nicola Omodei, David Coward for their useful advices.

References

- Abdo et al. 2009, Science, 323, 1688.
 Abdo et al. 2010, astro-ph/1002.3205 accepted in ApJ.
 Ando, S., Nakar, E. & Sari, R. 2008, ApJ 689, 1150.
 Atwood, W., et al. 2009, ApJ 697, 1071.
 Band, D. 2003, ApJ 588, 945.
 Band, D. et al. 2009, ApJ 701, 1673B.
 Bissaldi et al. 2009, astro-ph/0909.2470.
 Dermer, C. D. & Fryer, C. L. 2008, astro-ph/0909.3959.
 Dingus, B. 1995, Astrophysics and Space Science 231, 187.
 Drenhahn, G & Spruit, H.C. 2002, A&A 391, 1141.
 Ghisellini, Nava, & Ghirlanda 2010, MNRAS 144.
 Giuliani et al. 2008, A&A, 491.
 Giuliani et al. 2010, ApJ 708, L84.
 Gonzalez, M. M. et al. 2003, Nature, 424, 749.
 Gonzalez Sanchez, M. M. et al. 2005, Ph. D. Thesis, Univ. Wisconsin, Madison
 Gorosabel, J. et al. 2004, A&A 427, 87.
 Guetta, D., Spada, M. & Waxman E., 2001, ApJ, 557, 399.
 Guetta, D., Piran, T. & Waxman E., 2005, ApJ, 619, 412.
 Guetta, D., & Piran, T. 2007, JCAP 07, 3.
 Guidorzi, C., et al. 2004, ASPC 312, 39.
 Hurley, K. 1994, Nature 372, 652.
 Lyutikov, M. Pariev, V. I. & Blandford, R. D. 2003, ApJ 597, 998.
 Marisaldi, M. et al. 2009, astro-ph/0906.1446.
 Mészáros, P. 2006, Rep. Prog. Phys. 69, 2259.
 Paciesas, W., et al. 1999, ApJS, 122, 465.
 Panaitescu, A. & Kumar, P. 2007, MNRAS 376, 1065.
 Pe’er, A. & Waxman, E. 2004, ApJ 613, 448.
 Piran, T. 2004, Rev. Mod. Phys. 76, 1143.
 Porciani, C. & Madau, P. 2001, ApJ 548, 522.
 Schmidt, M., 1999, ApJ 559, L79.
 Stern, B. E. & Poutanen, J. 2004, MNRAS 352, L35.
 Waxman, E. 2003, Lect. Notes in Phys. 598, 393.

Table 2. GBM parameters for the bursts detected by Fermi.

GRB ¹	T_{90}^2 (s)	Fluence ³ (10^{-6} erg cm $^{-2}$)	PF ⁴ (ph s $^{-1}$ cm $^{-2}$)	Band ⁵ (keV)	Function ⁶	E_p^7 (keV)	α^8	β^9	θ^{10} (deg)	LAT ¹¹	$\nu f_\nu(1 \text{ MeV})^{12}$ (erg s $^{-1}$ cm $^{-2}$)	$\nu f_\nu(100 \text{ MeV})^{13}$ (erg s $^{-1}$ cm $^{-2}$)	z^{14}
080810	122.0	6.90e+00	1.85e+00	50 300	PL+HEC	313.5	-0.91	-1000	61	0	1.48e-08	0	3.35
080812	15.0	-1	-1	* *	PL+HEC	140.0	0.17	-1000	71	0	0	0	-1
080816A	70.0	1.86e+01	3.48e+00	50 300	PL+HEC	146.7	-0.57	-1000	55	0	6.70e-10	0	-1
080816B	5.0	-1	1.38e+00	25 1000	PL+HEC	1230.0	-0.37	-1000	70	0	0	0	-1
080817A	70.0	-1	-1	* *	*	-1	1000.00	-1000	80	0	0	0	-1
080817B	6.0	2.60e+00	-1	25 1000	SPL	-1	-17	-1000	68	0	4.16e-07	0	-1
080818A	50.0	2.26e+00	-1	50 300	SPL	-1	-1.57	-1000	68	0	0	0	-1
080818B	10.0	1.00e+00	-1	50 300	PL+HEC	80.0	-1.30	-1000	68	0	1.26e-10	0	-1
080823	46.0	4.10e+00	-1	50 300	PL+HEC	164.7	-1.20	-1000	77	0	4.06e-09	0	-1
080824	28.0	2.30e+00	-1	50 300	Band	100.0	-0.40	-2.10	17	0	3.92e-08	2.47e-08	-1
080825C	22.0	2.40e+01	-1	50 300	Band	155.0	-0.39	-2.34	60	1	3.99e-07	8.34e-08	-1
080830	45.0	4.60e+00	-1	50 300	Band	154.0	-0.59	-1.69	23	0	1.13e-07	4.69e-07	-1
080904	22.0	2.25e+00	3.50e+00	50 300	Band	35.0	0.00	-2.70	23	0	1.29e-08	5.13e-10	-1
080905B	159.0	4.10e-02	2.10e-01	20 1000	SPL	-1	-1.75	-1000	82	0	1.03e-10	0	2.37
080905C	28.0	4.60e+00	4.40e+00	25 1000	PL+HEC	78.8	-0.90	-1000	108	0	3.63e-12	0	-1
080906B	5.0	1.09e+01	2.20e+01	25 1000	Band	125.3	-0.07	-2.10	32	0	6.17e-07	3.89e-07	-1
080912	17.0	3.30e+00	4.10e+00	25 1000	SPL	-1	-1.74	-1000	56	0	8.18e-08	0	-1
080913B	140.0	2.20e+00	-1	50 300	PL+HEC	114.0	-0.69	-1000	71	0	3.19e-11	0	-1
080916A	60.0	1.50e+01	4.50e+00	25 1000	PL+HEC	109.0	-0.90	-1000	76	0	1.70e-10	0	0.69
080916C	100.9	2.40e+02	6.87e+00	10 10000	Band	566.0	-0.92	-2.28	48	1	5.77e-07	1.59e-07	4.2
080920	85.0	2.40e+00	1.29e+00	25 1000	SPL	-1	-1.42	-1000	16	0	1.86e-08	0	-1
080925	29.0	9.70e+00	-1	50 300	Band	120.0	-0.53	-2.26	38	0	1.24e-07	3.74e-08	-1
080927	25.0	5.70e+00	2.00e+00	25 1000	SPL	-1	-1.50	-1000	75	0	1.57e-07	0	-1
080928	87.0	1.50e+00	-1	50 300	SPL	-1	-1.80	-1000	-1	0	0	0	1.69
081003C	67.0	5.40e+00	-1	50 300	SPL	-1	-1.41	-1000	48	0	1.48e-07	0	-1
081006A	7.0	7.10e-01	-1	50 300	Band	1135.0	-0.77	-1.80	16	0	2.54e-07	6.37e-07	-1
081006B	9.0	7.30e-01	-1	50 300	SPL	-1	-1.30	-1000	3	0	1.85e-07	0	-1
081007A	12.0	1.20e+00	2.20e+00	25 900	SPL	-1	-2.10	-1000	116	0	3.72e-08	0	0.53
081009	13.0	8.30e+00	-1	8 1000	Band	20.7	0.20	-4.00	67	0	2.53e-10	2.53e-14	-1
081012	30.0	3.80e+00	2.00e+00	25 900	PL+HEC	360.0	-0.31	-1000	61	0	5.44e-08	0	-1
081021	25.0	5.30e+00	4.20e+00	10 1000	Band	117.0	0.11	-2.80	125	0	2.55e-08	6.42e-10	-1
081024C	65.0	4.00e+00	1.00e+00	50 300	Band	65.0	-0.60	-2.50	78	0	1.21e-08	1.21e-09	-1
081025	45.0	7.10e+00	4.50e+00	8 1000	Band	200.0	0.15	-2.05	-1	0	9.87e-08	7.84e-08	-1
081028B	20.0	2.00e+00	6.90e+00	10 1000	PL+HEC	70.0	-0.55	-1000	107	0	1.63e-14	0	-1

GRB	T_{90} (s)	Fluence (10^{-6} erg cm $^{-2}$)	PF (ph s $^{-1}$ cm $^{-2}$)	Band (keV)	Function	E_p (keV)	α	β	θ (deg)	LAT	$v f_{nu}$ (1 MeV) (erg s $^{-1}$ cm $^{-2}$)	$v f_{nu}$ (100 MeV) (erg s $^{-1}$ cm $^{-2}$)	z
081101B	8.0	1.60e+01	1.03e+01	8 1000	PL+HEC	550.0	-0.62	-1000	116	0	7.99e-07	0	-1
081102A	88.0	2.10e+00	-1	50 300	Band	72.0	0.44	-2.36	-1	0	1.16e-08	2.22e-09	3.04
081102B	2.2	1.12e+00	3.68e+00	8 1000	SPL	-1	-17	-1000	53	0	1.03e-06	0	-1
081107	2.2	1.64e+00	1.10e+01	8 1000	Band	65.0	0.25	-2.80	52	0	5.04e-08	1.27e-09	-1
081109A	45.0	6.53e+00	3.20e+00	8 1000	PL+HEC	240.0	-1.28	-1000	-1	0	1.92e-08	0	-1
081110	20.0	-1	-1	8 1000	*	-1	1000.00	-1000	67	0	0	0	-1
081118B	20.0	1.12e-01	6.70e-01	8 1000	Band	41.2	0.80	-2.14	41	0	7.07e-10	3.71e-10	-1
081120	12.0	2.70e+00	5.10e+00	8 1000	Band	44.0	0.40	-2.18	84	0	5.05e-08	2.20e-08	-1
081122A	26.0	9.60e+00	3.00e+01	8 1000	Band	158.6	-0.63	-2.24	21	0	8.14e-08	2.69e-08	-1
081124	35.0	9.50e-02	6.70e-01	8 1000	Band	22.8	-0.60	-2.83	86	0	7.57e-11	1.66e-12	-1
081125	15.0	4.91e+01	2.70e+01	8 1000	Band	221.0	0.14	-2.34	126	0	9.23e-07	1.93e-07	-1
081129	59.0	2.00e+01	1.40e+01	8 1000	Band	150.0	-0.50	-1.84	118	0	1.31e-07	2.73e-07	-1
081130B	12.0	1.30e+00	1.80e+00	50 300	PL+HEC	152.0	-0.77	-1000	66	0	1.10e-09	0	-1
081204C	4.7	1.48e+00	7.20e+00	8 1000	SPL	-1	-1.40	-1000	56	0	3.03e-07	0	-1
081206A	24.0	4.00e+00	2.40e+00	8 1000	Band	151.0	0.13	-2.20	102	0	4.88e-08	1.94e-08	-1
081206B	10.0	-1	-1	* *	*	-1	1000.00	-1000	82	0	0	0	-1
081206C	20.0	1.19e+00	7.60e-01	50 300	SPL	-1	-1.35	-1000	71	0	0	0	-1
081207	153.0	1.06e+02	-1	10 1000	Band	639.0	-0.65	-2.41	56	0	8.91e-07	1.35e-07	-1
081215A	7.7	5.44e+01	6.89e+01	8 1000	Band	304.0	-0.58	-2.07	86	1	1.31e-06	9.69e-07	-1
081215B	90.0	2.80e+00	-1	50 300	PL+HEC	139.0	-0.14	-1000	112	0	8.24e-11	0	-1
081217	39.0	1.00e+01	4.00e+00	8 1000	Band	167.0	-0.61	-2.70	54	0	7.20e-08	2.87e-09	-1
081221	40.0	3.70e+01	3.30e+01	8 1000	Band	77.0	-0.42	-2.91	78	0	4.87e-08	7.37e-10	-1
081222	30.0	1.35e+01	1.48e+01	8 1000	Band	134.0	-0.55	-2.10	50	0	3.08e-07	1.94e-07	2.77
081224	50.0	-1	-1	* *	*	-1	1000.00	-1000	16	0	0	0	-1
081225	42.0	2.45e+00	6.00e-01	50 300	SPL	-1	-1.51	-1000	55	0	0	0	-1
081226C	60.0	2.32e+00	4.50e+00	8 1000	PL+HEC	82.0	-14	-1000	54	0	1.54e-11	0	-1
081231	29.0	1.20e+01	1.53e+00	8 1000	Band	152.3	-0.80	-2.03	20	0	8.25e-08	7.19e-08	-1
090107B	24.1	1.75e+00	3.68e+00	8 1000	PL+HEC	106.1	-0.68	-1000	-1	0	9.11e-12	0	-1
090109	5.0	1.21e+00	2.76e+00	8 1000	SPL	-1	-1.50	-1000	62	0	1.62e-07	0	-1
090112A	65.0	5.20e+00	7.00e+00	8 1000	Band	150.0	-0.94	-2.01	4	0	6.23e-08	5.95e-08	-1
090112B	12.0	5.40e+00	1.40e+01	8 1000	Band	139.0	-0.75	-2.43	95	0	1.01e-07	1.39e-08	-1
090117A	21.0	1.80e+00	9.60e+00	8 1000	Band	25.0	-0.40	-2.50	51	0	1.26e-08	1.26e-09	-1
090117B	27.0	2.10e+00	4.60e+00	8 1000	SPL	-1	-1.55	-1000	49	0	3.95e-08	0	-1
090117C	86.0	1.10e+01	4.20e+00	8 1000	Band	247.0	-1	-2.10	54	0	1.05e-07	6.65e-08	-1

GRB	T_{90} (s)	Fluence (10^{-6} erg cm $^{-2}$)	PF (ph s $^{-1}$ cm $^{-2}$)	Band (keV)	Function	E_p (keV)	α	β	θ (deg)	LAT	$\nu f_{nu}(1 \text{ MeV})$ (erg s $^{-1}$ cm $^{-2}$)	$\nu f_{nu}(100 \text{ MeV})$ (erg s $^{-1}$ cm $^{-2}$)	z
090126B	10.8	1.25e+00	4.90e+00	8 1000	PL+HEC	47.5	-0.99	-1000	18	0	1.85e-15	0	-1
090129	17.2	5.60e+00	8.00e+00	8 1000	Band	123.2	-1.39	-1.98	22	0	9.45e-08	1.04e-07	-1
090131	36.4	2.23e+01	4.79e+01	8 1000	Band	58.4	-1.27	-2.26	40	0	7.33e-08	2.21e-08	-1
090202	66.0	8.65e+00	7.77e+00	8 1000	PL+HEC	570.0	-1.31	-1000	55	0	1.66e-07	0	-1
090207	10.0	4.01e+00	1.88e+00	8 1000	SPL	-1	-1.59	-1000	45	0	1.10e-07	0	-1
090217	32.8	3.08e+01	1.12e+01	8 1000	Band	610.0	-0.85	-2.86	34	1	6.62e-07	9.74e-09	-1
090222	18.0	2.19e+00	1.10e+00	8 1000	Band	147.9	-0.97	-2.56	80	0	1.71e-08	1.30e-09	-1
090227A	50.0	9.00e+00	4.57e+00	8 1000	Band	1357.0	-0.92	-3.60	21	0	4.00e-07	4.30e-10	-1
090228B	7.2	9.96e-01	2.53e+00	8 1000	PL+HEC	147.8	-0.70	-1000	20	0	4.01e-10	0	-1
090301B	28.0	2.69e+00	4.40e+00	8 1000	Band	427.0	-0.98	-1.93	56	0	2.21e-07	3.05e-07	-1
090306C	38.8	9.00e-01	2.40e+00	8 1000	Band	87.0	-0.32	-2.28	14	0	1.52e-08	4.19e-09	-1
090307B	30.0	1.70e+00	1.80e+00	8 1000	PL+HEC	212.0	-0.70	-1000	83	0	2.71e-09	0	-1
090308B	2.1	3.46e+00	1.42e+01	8 1000	PL+HEC	710.3	-0.54	-1000	50	0	1.06e-06	0	-1
090309B	60.0	4.70e+00	4.43e+00	8 1000	PL+HEC	197.0	-1.52	-1000	26	0	1.38e-08	0	-1
090310	125.2	2.15e+00	4.40e+00	8 1000	PL+HEC	279.0	-0.65	-1000	77	0	4.02e-08	0	-1
090319	67.7	7.47e+00	3.85e+00	8 1000	PL+HEC	187.3	0.90	-1000	27	0	4.95e-11	0	-1
090320A	10.0	-1	-1	8 1000	*	-1	1000.00	-1000	60	0	0	0	-1
090320B	52.0	1.10e+00	1.20e-01	8 1000	PL+HEC	72.0	-1.10	-1000	101	0	7.16e-13	0	-1
090320C	4.0	-1	-1	8 1000	*	-1	1000.00	-1000	40	0	0	0	-1
090323	70.0	1.00e+02	1.23e+01	8 1000	PL+HEC	697.0	-0.89	-1000	-1	1	6.46e-07	0	3.57
090326	11.2	8.60e-01	-1	8 1000	PL+HEC	75.0	-0.86	-1000	103	0	4.17e-13	0	-1
090327	24.0	3.00e+00	3.50e+00	8 1000	Band	89.7	-0.39	-2.90	66	0	1.09e-08	1.72e-10	-1
090328A	100.0	8.09e+01	1.85e+01	8 1000	Band	653.0	-0.93	-2.20	-1	1	1.40e-06	5.57e-07	0.74
090330	80.0	1.14e+01	6.80e+00	8 1000	Band	246.0	-0.99	-2.68	50	0	7.45e-08	3.25e-09	-1
090403	16.0	-1	-1	** *	*	-1	1000.00	-1000	42	0	0	0	-1
090409	20.0	6.14e-01	1.36e+00	8 1000	PL+HEC	137.0	1.20	-1000	90	0	8.53e-14	0	-1
090411A	24.6	8.60e+00	3.25e+00	8 1000	Band	141.0	-0.88	-1.82	59	0	1.57e-07	3.60e-07	-1
090411B	18.7	8.00e+00	7.40e+00	8 1000	Band	189.0	-0.80	-2.00	111	0	1.09e-07	1.09e-07	-1
090422	10.0	1.00e+00	7.80e+00	8 1000	SPL	-1	1.81	-1000	29	0	2.89e-07	0	-1
090423	12.0	1.10e+00	3.30e+00	8 1000	PL+HEC	82.0	-0.77	-1000	75.6	0	8.96e-13	0	8.10
090424	52.0	5.20e+01	1.37e+02	8 1000	Band	177.0	0.90	-2.90	71	0	1.13e-07	1.79e-09	0.54
090425	72.0	1.30e+01	1.40e+01	8 1000	Band	69.0	-1.29	-2.03	105	0	1.28e-07	1.12e-07	-1
090426B	3.8	5.20e-01	-1	8 1000	SPL	-1	-1.60	-1000	56	0	4.75e-08	0	-1
090426C	12.0	3.10e+00	6.80e+00	8 1000	Band	295.0	-1.29	-1.98	69	0	9.65e-08	1.06e-07	-1

GRB	T_{90} (s)	Fluence (10^{-6} erg cm $^{-2}$)	PF (ph s $^{-1}$ cm $^{-2}$)	Band (keV)	Function	E_p (keV)	α	β	θ (deg)	LAT	$v f_{nu}(1 \text{ MeV})$ (erg s $^{-1}$ cm $^{-2}$)	$v f_{nu}(100 \text{ MeV})$ (erg s $^{-1}$ cm $^{-2}$)	z
090427B	7.0	8.00e-01	-1	8 1000	SPL	-1	-1.10	-1000	14	0	1.19e-07	0	-1
090427C	12.5	1.60e+00	-1	8 1000	PL+HEC	75.0	0.35	-1000	81	0	7.59e-18	0	-1
090428A	8.0	9.90e-01	1.23e+01	8 1000	Band	85.0	-0.40	-2.70	96	0	3.13e-08	1.25e-09	-1
090428B	30.0	5.20e+00	1.01e+01	8 1000	Band	53.0	-1.81	-2.17	101	0	3.25e-08	1.49e-08	-1
090429C	13.0	3.70e+00	6.70e+00	8 1000	SPL	-1	-1.43	-1000	112	0	1.73e-07	0	-1
090429D	11.0	1.60e+00	8.60e-01	8 1000	SPL	223.0	-0.87	-1000	33	0	1.27e-07	0	-1
090502	66.2	3.50e-02	6.20e+00	8 1000	PL+HEC	63.2	-1.10	-1000	77	0	3.68e-15	0	-1
090509	295.0	8.40e+00	3.10e+00	8 1000	SPL	-1	-1.55	-1000	75	0	2.18e-10	0	-1
090510B	7.0	-1	-1	* *	*	-1	1000.00	-1000	100	0	0	0	-1
090511	14.0	1.80e+00	2.50e+00	8 1000	PL+HEC	391.0	-0.95	-1000	67	0	4.26e-08	0	-1
090513A	23.0	6.80e+00	2.70e+00	8 1000	PL+HEC	850.0	-0.90	-1000	89	0	1.91e-07	0	-1
090514	49.0	8.10e+00	7.60e+00	8 1000	SPL	-1	-1.92	-1000	19	0	3.47e-08	0	-1
090516A	350.0	2.30e+01	5.30e+00	8 1000	Band	51.4	-13	-2.10	20	0	1.49e-08	9.41e-09	4.11
090516B	350.0	3.00e+01	4.00e+00	8 1000	PL+HEC	327.0	-11	-1000	45	0	3.38e-08	0	-1
090516C	15.0	4.00e+00	7.70e+00	8 1000	Band	38.0	-0.44	-1.81	69	0	8.74e-08	2.10e-07	-1
090518A	9.0	1.60e+00	4.70e+00	8 1000	SPL	-1	-1.59	-1000	53	0	8.38e-08	0	-1
090518B	12.0	2.20e+00	5.60e+00	8 1000	PL+HEC	127.0	-0.74	-1000	90	0	3.00e-10	0	-1
090519B	87.0	1.40e+00	5.02e+00	8 1000	SPL	-1	-1.63	-1000	18	0	1.74e-07	0	-1
090520C	4.9	3.54e+00	4.47e+00	8 1000	Band	204.2	-0.73	-1.96	71	0	2.75e-07	3.31e-07	-1
090520D	12.0	4.00e+00	4.10e+00	8 1000	Band	46.3	-0.99	-3.25	66	0	3.32e-09	1.05e-11	-1
090522	22.0	1.20e+00	3.50e+00	8 1000	PL+HEC	75.8	-13	-1000	53	0	1.97e-12	0	-1
090524	72.0	1.85e+01	1.41e+01	8 1000	Band	82.6	-1	-2.30	63	0	3.86e-08	9.70e-09	-1
090528A	68.0	9.30e+00	7.60e+00	8 1000	PL+HEC	99.0	-1.70	-1000	81	0	9.53e-09	0	-1
090528B	102.0	4.65e+01	1.47e+01	8 1000	Band	172.0	-1.10	-2.30	65	0	1.56e-07	3.91e-08	-1
090529B	5.1	3.40e-01	4.10e+00	8 1000	Band	142.0	-0.70	-2.00	36	0	1.42e-08	1.42e-08	-1
090529C	10.4	3.10e+00	2.50e+01	8 1000	Band	188.0	-0.84	-2.10	69	0	8.64e-08	5.45e-08	-1
090530B	194.0	5.90e+01	1.08e+01	8 1000	Band	67.0	-0.71	-2.42	84	0	5.92e-08	8.55e-09	-1
090602	16.0	5.70e+00	3.62e+00	8 1000	PL+HEC	503.0	-0.56	-1000	112	0	1.84e-07	0	-1
090606	60.0	3.19e+00	2.41e+00	8 1000	SPL	-1	-1.63	-1000	128	0	8.15e-08	0	-1
090608	61.0	3.20e+00	2.70e+00	8 1000	SPL	-1	-1.83	-1000	93	0	2.50e-08	0	-1
090610A	6.5	7.32e-01	9.40e-01	8 1000	SPL	-1	-1.30	-1000	70	0	8.42e-08	0	-1
090610B	202.5	4.13e+00	1.54e+00	8 1000	SPL	-1	-1.66	-1000	91	0	8.41e-10	0	-1
090610C	18.1	8.54e-01	1.12e+00	8 1000	SPL	-1	-1.62	-1000	104	0	3.14e-08	0	-1
090612	58.0	2.37e+00	1.63e+00	8 1000	Band	357.0	-0.60	-1.90	56	0	1.75e-07	2.78e-07	-1

GRB	T_{90} (s)	Fluence (10^{-6} erg cm $^{-2}$)	PF (ph s $^{-1}$ cm $^{-2}$)	Band (keV)	Function	E_p (keV)	α	β	θ (deg)	LAT	$\nu f_{nu}(1 \text{ MeV})$ (erg s $^{-1}$ cm $^{-2}$)	$\nu f_{nu}(100 \text{ MeV})$ (erg s $^{-1}$ cm $^{-2}$)	z
090616	2.7	2.23e-01	2.08e+00	8 1000	SPL	-1	-1.27	-1000	68	0	2.62e-07	0	-1
090618	155.0	2.70e+02	7.34e+01	8 1000	Band	155.5	-1.26	-2.50	133	0	2.75e-07	2.75e-08	0.54
090620	16.5	6.60e+00	7.00e+00	8 1000	Band	156.0	-0.40	-2.44	60	0	7.19e-08	9.48e-09	-1
090621A	294.0	4.40e+00	1.92e+00	8 1000	Band	56.0	-1.10	-2.12	12	0	1.59e-08	9.15e-09	-1
090621C	59.9	1.80e+00	2.29e+00	8 1000	PL+HEC	148.0	-1.40	-1000	52	0	1.79e-09	0	-1
090621D	39.9	1.34e+00	1.74e+00	8 1000	SPL	-1	-1.66	-1000	79	0	2.63e-08	0	-1
090623	72.2	9.60e+00	3.30e+00	8 1000	Band	428.0	-0.69	-2.30	73	0	8.35e-08	2.10e-08	-1
090625A	51.0	8.80e-01	5.00e-01	8 1000	PL+HEC	198.0	-0.60	-1000	13	0	7.18e-10	0	-1
090625B	13.6	1.04e+00	1.87e+00	8 1000	Band	100.0	-0.40	-2.00	125	0	3.62e-08	3.62e-08	-1
090626	70.0	3.50e+01	1.79e+01	8 1000	Band	175.0	-1.29	-1.98	15	1	1.43e-07	1.57e-07	-1
090630	5.1	5.10e-01	2.78e+00	8 1000	Band	71.0	-1.50	-2.30	75	0	1.32e-08	3.30e-09	-1
090701	12.0	4.50e-01	2.10e+00	8 1000	SPL	-1	1.84	-1000	13	0	1.44e-07	0	-1
090703	9.0	6.80e-01	1.00e+00	8 1000	SPL	-1	-1.72	-1000	25	0	2.76e-08	0	-1
090704	70.0	5.80e+00	1.20e+00	8 1000	PL+HEC	233.7	-1.13	-1000	77	0	6.15e-09	0	-1
090706	100.0	1.50e+00	1.24e+00	8 1000	SPL	-1	-2.16	-1000	20	0	4.90e-09	0	-1
090708	18.0	4.00e-01	1.00e+00	8 1000	PL+HEC	47.5	-1.29	-1000	55	0	4.90e-14	0	-1
090709B	32.0	1.30e+00	2.00e+00	8 1000	PL+HEC	130.0	-11	-1000	35	0	1.71e-10	0	-1
090711	100.0	1.17e+01	4.20e+00	8 1000	PL+HEC	210.0	-1.30	-1000	13	0	8.06e-09	0	-1
090712	72.0	4.20e+00	6.30e-01	8 1000	PL+HEC	505.0	-0.68	-1000	33	0	1.96e-08	0	-1
090713	113.0	3.70e+00	1.60e+00	8 1000	PL+HEC	99.0	-0.34	-1000	63	0	3.98e-13	0	-1
090717A	70.0	4.50e-01	7.80e+00	8 1000	Band	120.0	-0.88	-2.33	70	0	4.66e-09	1.02e-09	-1
090718B	28.0	2.52e+01	3.20e+01	8 1000	Band	184.0	-1.18	-2.59	76	0	1.24e-07	8.19e-09	-1
090719	16.0	4.83e+01	3.78e+01	8 1000	Band	254.0	-0.68	-2.92	88	0	4.55e-07	6.57e-09	-1
090720A	7.0	2.90e+00	1.09e+01	8 1000	PL+HEC	117.5	-0.75	-1000	113	0	2.14e-10	0	-1
090720B	20.0	1.06e+01	1.09e+01	8 1000	Band	924.0	-1	-2.43	56	0	2.96e-07	3.97e-08	-1
090807B	3.0	1.02e+00	1.09e+01	8 1000	Band	37.0	-0.60	-2.40	45	0	4.65e-08	7.38e-09	-1
090809B	15.0	2.26e+01	2.36e+01	8 1000	Band	198.0	-0.85	-2.02	81	0	4.95e-07	4.51e-07	-1
090813	9.0	3.50e+00	1.44e+01	8 1000	Band	95.0	-1.25	-2.00	35.3	0	9.45e-08	9.45e-08	-1
090815A	200.0	3.40e+00	1.90e+00	8 1000	SPL	-1	-1.50	-1000	87	0	6.29e-08	0	-1
090815B	30.0	5.05e+00	1.44e+01	8 1000	Band	18.6	-1.82	-2.70	82	0	6.71e-09	2.67e-10	-1
090817	220.0	7.30e+00	3.80e+00	8 1000	Band	115.0	-1.10	-2.20	82	0	6.47e-09	2.58e-09	-1
090820A	60.0	6.60e+01	5.80e+01	8 1000	Band	215.0	-0.69	-2.61	108	0	3.64e-07	2.19e-08	-1

GRB	T_{90} (s)	Fluence (10^{-6} erg cm $^{-2}$)	PF (ph s $^{-1}$ cm $^{-2}$)	Band (keV)	Function	E_p (keV)	α	β	θ (deg)	LAT	νf_{nu} (1 MeV) (erg s $^{-1}$ cm $^{-2}$)	νf_{nu} (100 MeV) (erg s $^{-1}$ cm $^{-2}$)	z
090820B	11.2	1.16e+00	6.10e+00	8 1000	PL+HEC	38.8	-1.44	-1000	32	0	2.10e-13	0	-1
090826	8.5	1.26e+00	3.28e+00	8 1000	PL+HEC	172.0	-0.96	-1000	35	0	1.55e-09	0	-1
090828	100.0	2.52e+01	1.62e+01	8 1000	Band	136.5	-1.23	-2.12	95	0	5.50e-08	3.16e-08	-1
090829A	85.0	1.02e+02	5.15e+01	8 1000	Band	183.0	-1.44	-2.10	47	0	2.44e-07	1.54e-07	-1
090829B	100.0	6.40e+00	3.20e+00	8 1000	Band	143.0	-0.70	-2.40	42	0	3.39e-08	5.38e-09	-1
090831	69.1	1.66e+01	9.40e+00	8 1000	Band	243.8	-1.52	-1.96	107	0	9.92e-08	1.19e-07	-1
090902B	21.0	3.74e+02	4.61e+01	50 10000	Band	798.0	-0.61	-3.87	52	1	7.16e-06	8.88e-10	1.82
090904B	71.0	2.44e+01	9.80e+00	8 1000	Band	106.3	-1.26	-2.18	113	0	6.20e-08	2.71e-08	-1
090910	62.0	9.20e+00	2.30e+00	8 1000	Band	274.8	-0.90	-2.00	107	0	6.32e-08	6.32e-08	-1
090922A	92.0	1.14e+01	1.56e+01	8 1000	Band	139.3	-0.77	-2.28	19	0	2.22e-07	6.11e-08	-1
090925	50.0	9.46e+00	4.20e+00	8 1000	Band	156.0	-0.60	-1.91	116	0	1.59e-07	2.41e-07	-1
090926A	20.0	1.45e+02	8.08e+01	8 1000	Band	268.0	-0.69	-2.34	52	1	1.85e-06	3.84e-07	2.11
090926B	81.0	8.70e+00	-1	10 1000	PL+HEC	91.0	-0.13	-1000	100	0	6.54e-14	0	1.24
090929A	8.5	1.06e+01	1.09e+01	8 1000	PL+HEC	610.9	-0.52	-1000	122	0	9.81e-07	0	-1
091003A	21.1	3.76e+01	3.18e+01	8 1000	Band	486.2	-1.13	-2.64	13	1	4.93e-07	2.59e-08	0.90
091010	8.1	1.09e+01	4.09e+01	8 1000	PL+HEC	150.0	-1.11	-1000	55.7	0	1.72e-08	0	-1
091020	37.0	1.00e+01	7.40e+00	8 1000	Band	47.9	0.20	-1.70	118	0	1.47e-07	5.84e-07	1.71
091024	1080.0	-1	-1	* *	*	400.0	1000.00	-1000	14	0	0	0	1.09
091030	160.0	3.03e+01	9.58e+00	8 1000	Band	507.0	-0.88	-2.20	100	0	2.92e-07	1.16e-07	-1
091031	35.0	2.05e+01	7.50e+00	8 1000	Band	503.1	-0.91	-2.34	22	1	2.09e-07	4.36e-08	-1
091102A	7.3	2.10e+00	2.90e+00	8 1000	SPL	-1	-1.24	-1000	94	0	3.20e-07	0	-1
091112	40.0	9.70e+00	-1	10 1000	PL+HEC	750.0	-1.13	-1000	82	0	1.80e-07	0	-1
091120	52.0	3.02e+01	2.13e+01	8 1000	Band	124.0	-1.15	-2.98	45	0	3.50e-08	3.83e-10	-1
091123	650.0	4.07e+01	6.10e+00	8 1000	PL+HEC	101.3	-18	-1000	106	0	5.65e-11	0	-1
091127	9.0	1.87e+01	4.69e+01	8 1000	Band	36.0	-1.27	-2.20	25	0	2.64e-07	1.05e-07	0.49
091128	97.0	3.76e+01	9.30e+00	8 1000	Band	177.4	-0.99	-3.90	96	0	1.83e-08	2.89e-12	-1
091208B	15.0	5.80e+00	3.24e+01	8 1000	Band	124.0	-1.44	-2.32	56	0	6.13e-08	1.40e-08	1.06
091221	32.0	1.38e+01	5.10e+00	8 1000	Band	207.0	-0.69	-2.30	53	0	1.03e-07	2.59e-08	-1
090530B	194.0	5.90e+01	1.08e+01	8 1000	Band	67.0	-0.71	-2.42	84	0	5.92e-08	8.55e-09	-1

GRB	T_{90} (s)	Fluence (10^{-6} erg cm $^{-2}$)	PF (ph s $^{-1}$ cm $^{-2}$)	Band (keV)	Function	E_p (keV)	α	β	θ (deg)	LAT	$\nu f_{nu}(1 \text{ MeV})$ (erg s $^{-1}$ cm $^{-2}$)	$\nu f_{nu}(100 \text{ MeV})$ (erg s $^{-1}$ cm $^{-2}$)	z
100111A	12.0	1.50e+00	3.50e+00	8 1000	SPL	-1	-1.66	-1000	32	0	7.71e-08	0	-1
100116A	110.0	3.36e+01	-1	8 10000	PL+HEC	1240.0	-12	-1000	29	1	6.39e-10	0	-1
100122A	6.6	1.00e+01	1.04e+01	8 1000	Band	45.6	-0.98	-2.31	45	0	4.18e-08	1.00e-08	-1
100130A	106.0	8.21e+00	5.90e+00	8 1000	PL+HEC	100.5	-0.97	-1000	51	0	3.36e-11	0	-1
100130B	90.0	1.34e+01	3.72e+00	8 1000	PL+HEC	208.0	-1.22	-1000	89	0	7.89e-09	0	-1
100131A	6.2	7.72e+00	3.38e+01	8 1000	Band	132.1	-0.63	-2.21	27	0	3.79e-07	1.44e-07	-1
100205B	13.6	1.41e+00	2.98e+00	8 1000	PL+HEC	124.2	-0.47	-1000	102	0	4.12e-11	0	-1
100212A	2.3	3.81e-01	3.16e+00	8 1000	PL+HEC	159.3	-1.15	-1000	15	0	9.60e-09	0	-1
100218A	30.8	2.58e+00	1.40e+00	8 1000	Band	131.6	-0.14	-2.00	37	0	2.50e-08	2.50e-08	-1

Notes. ⁽¹⁾ GRB name.

⁽²⁾ The duration of the GRB.

⁽³⁾ GRB fluence in the energy interval specified in Col. 5 (set to -1 when value is not available)

⁽⁴⁾ GRB peak flux (set to -1 when value is not available)

⁽⁵⁾ Energy band for the fluence determination

⁽⁶⁾ Method used to fit the spectra (Band=broken power law, SPL=single power law, PL+HEC=power law and exponential cutoff)

⁽⁷⁾ Peak energy (set to -1 when not available)

⁽⁸⁾ The α spectral index (set to 1000 when not available).

⁽⁹⁾ The β spectral index (set to -1000 when not available).

⁽¹⁰⁾ The angle, θ , from the LAT boresight, in deg (set to -1 when not available)

⁽¹¹⁾ LAT detection (1 = YES, 0 = NO)

⁽¹²⁾ The flux at \sim MeV (set zero when not available).

⁽¹³⁾ The flux at \sim 100 MeV obtained by extrapolating to high energy the \sim 1 MeV spectrum (set zero when not available).

⁽¹⁴⁾ The redshift (equal to -1 if not measured)